Supporting Information

Elucidating the Secondary Effect in Lewis Acid Mediated Anodic Shift of Electrochemical Oxidation of a Cu(II) Complex with N_2O_2 Donor Unsymmetrical Ligand

Souvik Maity,[†] Soumavo Ghosh,*[,†] and Ashutosh Ghosh*[,†]

[†]Department of Chemistry, University College of Science, University of Calcutta, 92, A. P. C. Road, Kolkata 700009, India, Email: ghosh_59@yahoo.com (A.G.), sanju.chem08@gmail.com (S.G.)

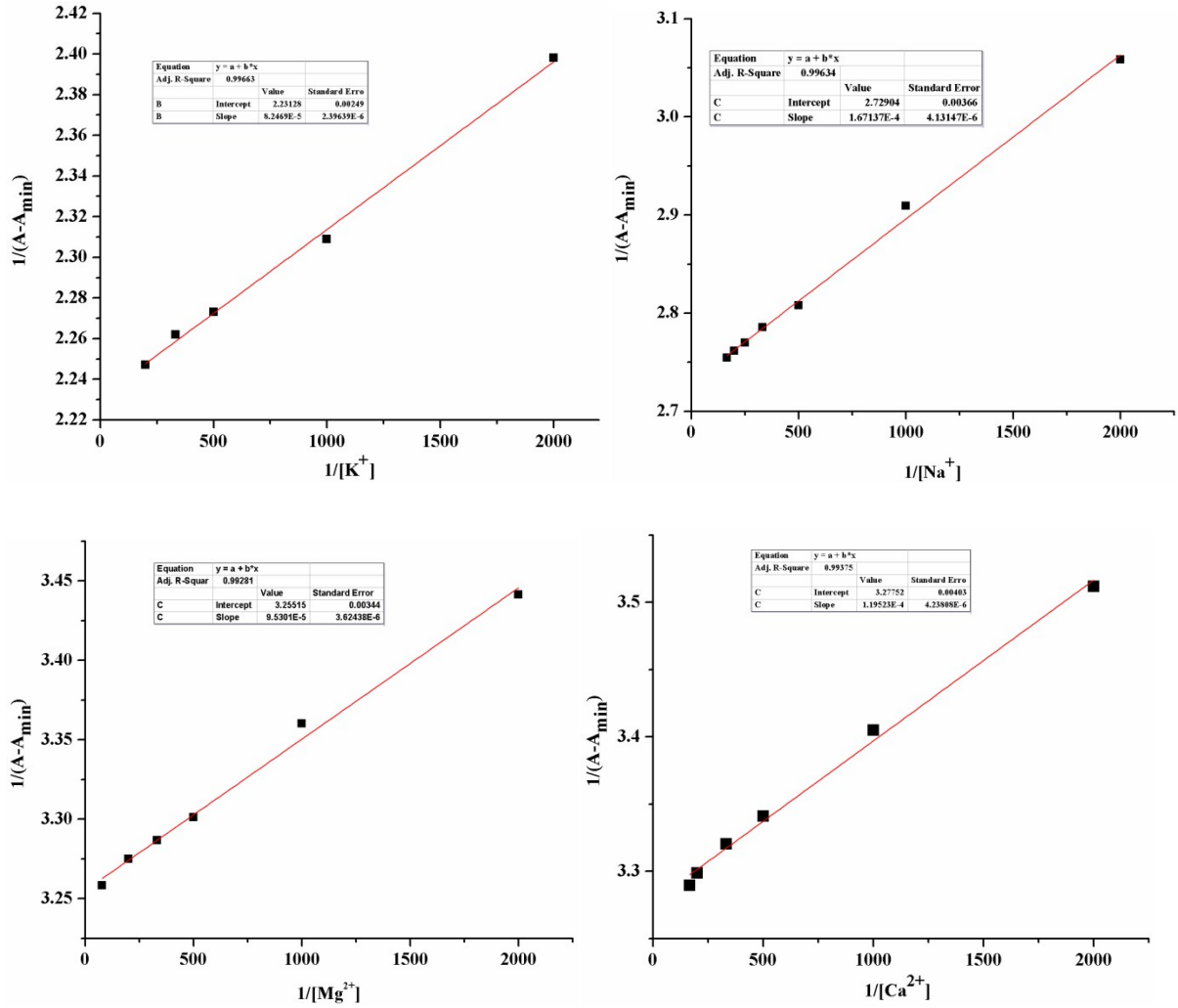

Fig. S1. Benesi−Hilderbrand plot for [CuL] + K^+ (upper panel left side), [CuL] + Na^+ (upper panel right side), [CuL] + Mg^{2+} (lower panel left side) and [CuL] + Ca^{2+} (lower panel right side) complex formation.

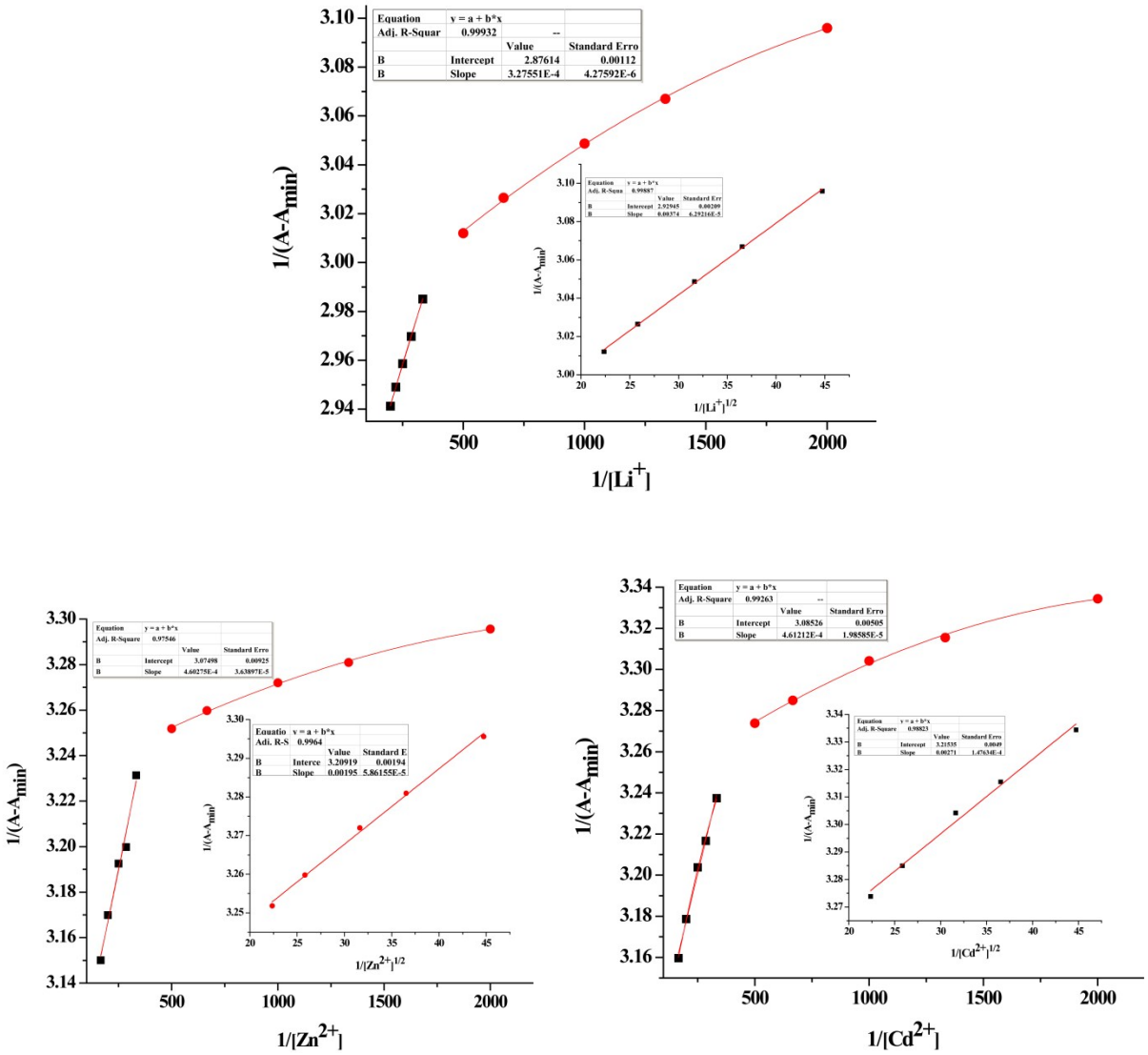

Fig. S2. Benesi−Hilderbrand plot for [CuL] + Li^{+} (upper panel), [CuL] + Zn^{2+} (lower panel left side) and [CuL] + Cd^{2+} (lower panel right side) complex formation.

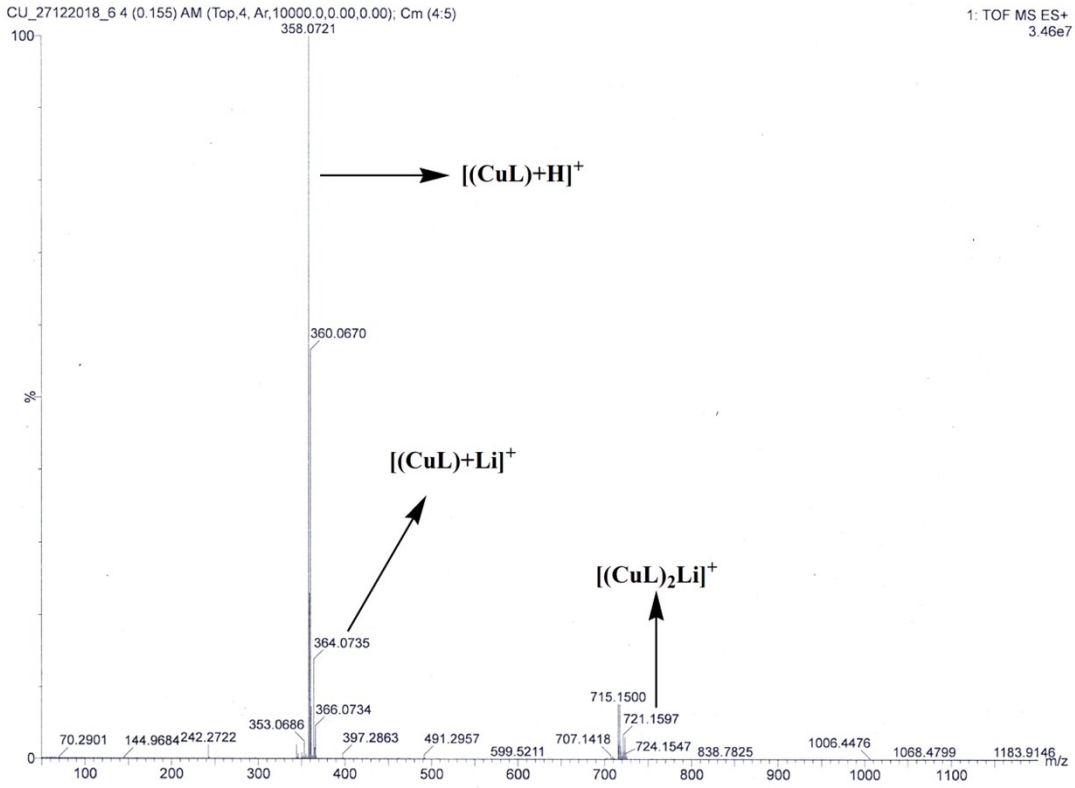

Fig. S3. Representative ESI mass spectrum of [CuL]–Li^{+} mixture in acetonitrile.

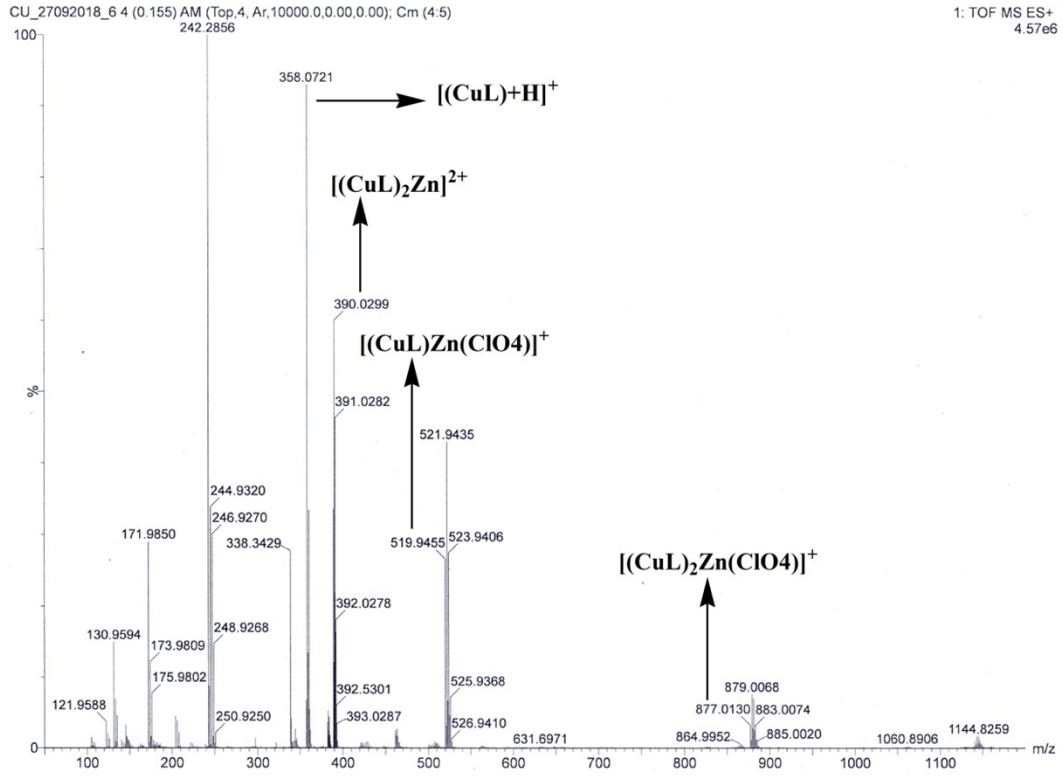

Fig. S4. Representative ESI mass spectrum of [CuL]–Zn^{2+} mixture in acetonitrile.

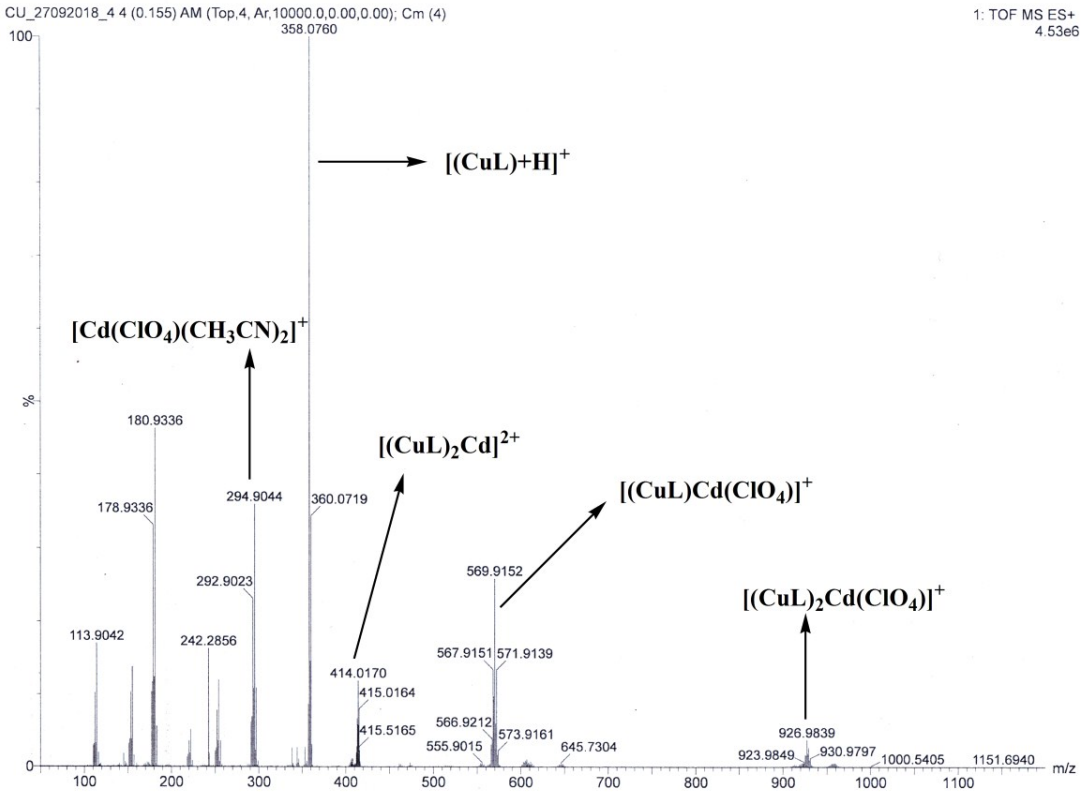

Fig. S5. Representative ESI mass spectrum of [CuL]–Cd^{2+} mixture in acetonitrile.

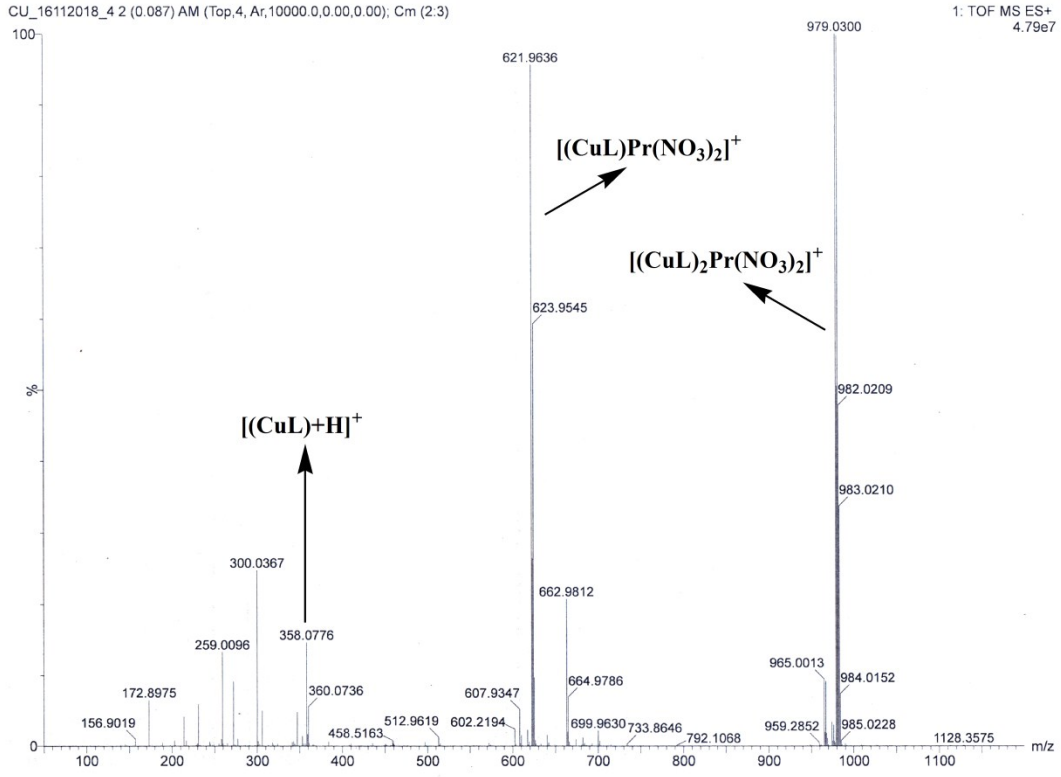

Fig. S6. Representative ESI mass spectrum of [CuL]–Pr^{3+} mixture in acetonitrile.

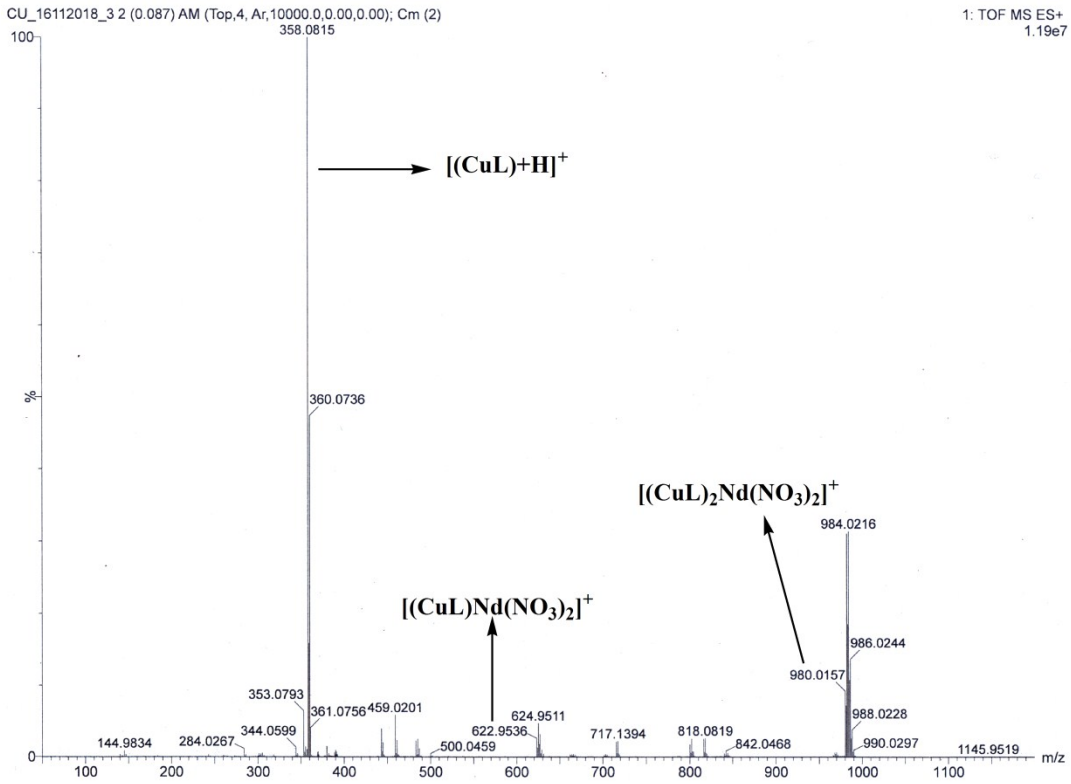

Fig. S7. Representative ESI mass spectrum of [CuL]–Nd^{3+} mixture in acetonitrile.

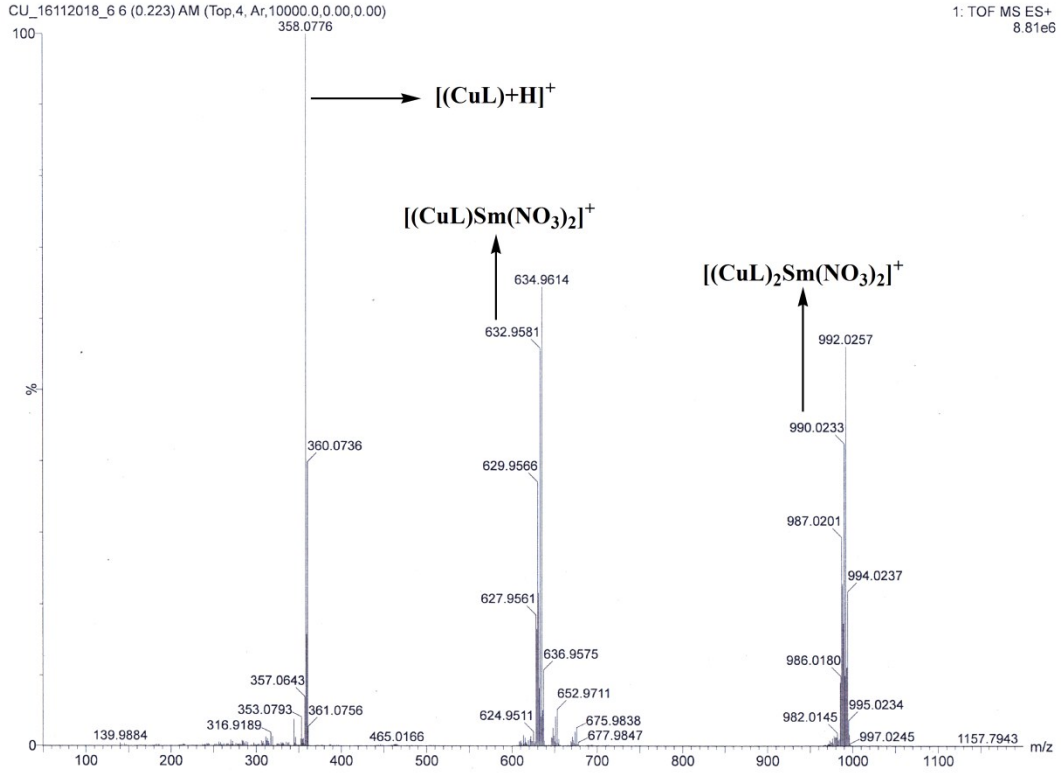

Fig. S8. Representative ESI mass spectrum of [CuL]–Sm^{3+} mixture in acetonitrile.

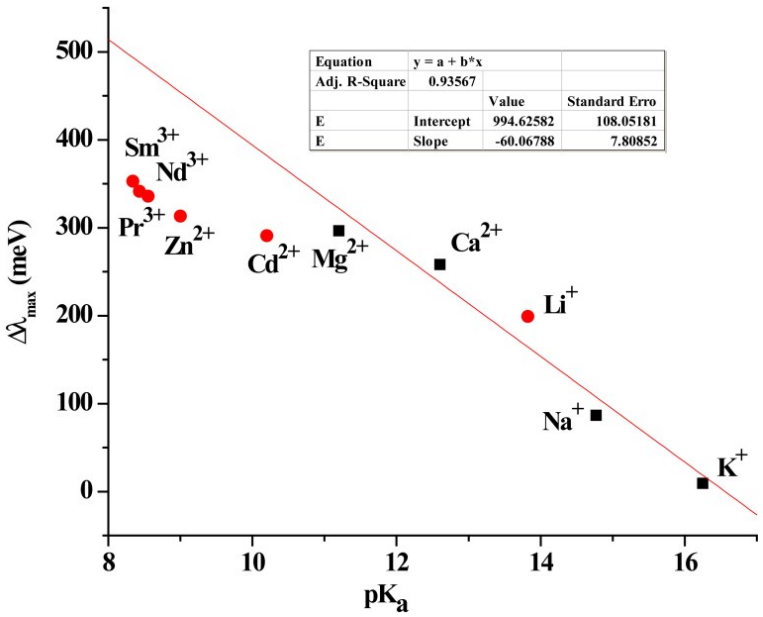

Fig. S9. Dependence of LMCT energy bands on pK_a of M'(aqua)$^{n+}$ ion as a measure of its Lewis acidity in presence of 100 equivalent of M′X_n salts.

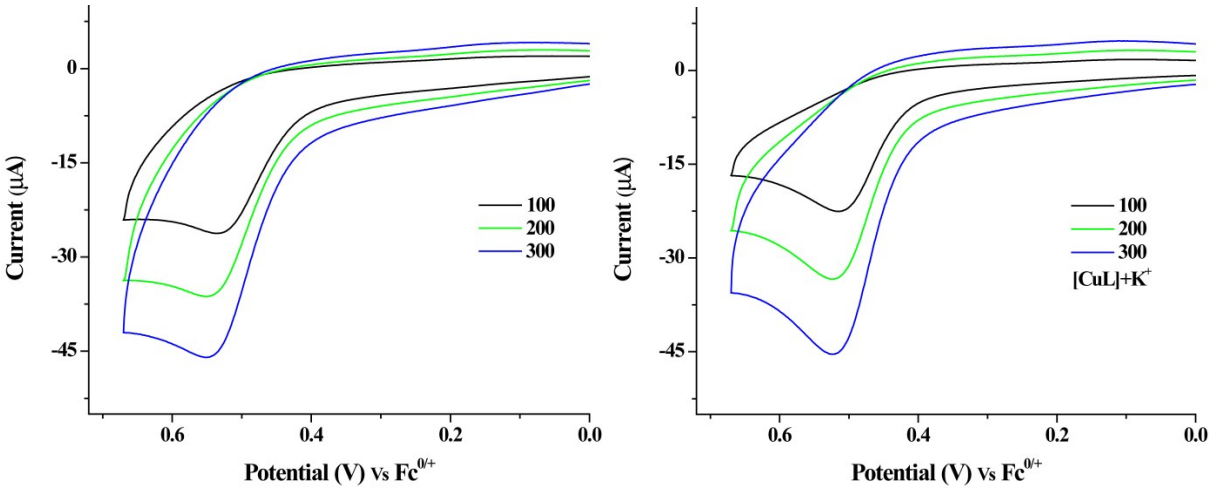

Fig. S10. Potential scan of unbound [CuL] and [CuL]+K^+ upto first oxidation step.

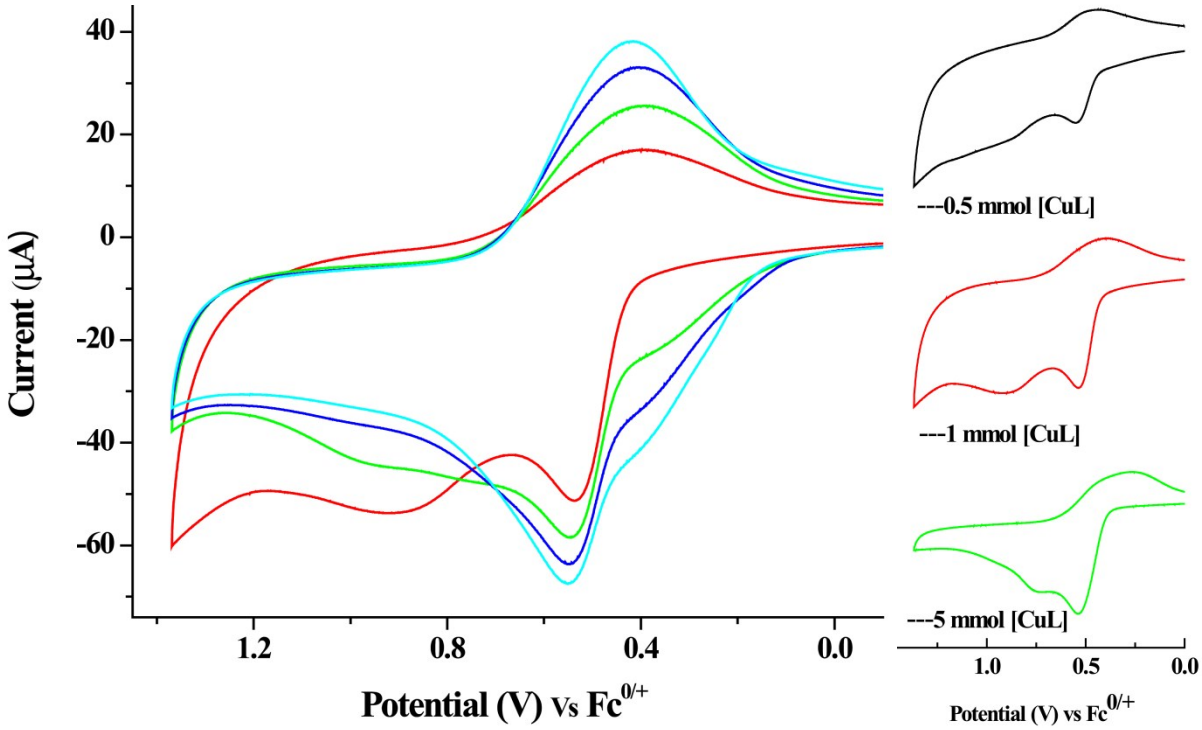

Fig. S11. Left: Multicycle CV of [CuL]. Right: CV of [CuL] at different concentration at 300 mV/S scan rate in acetonitrile.

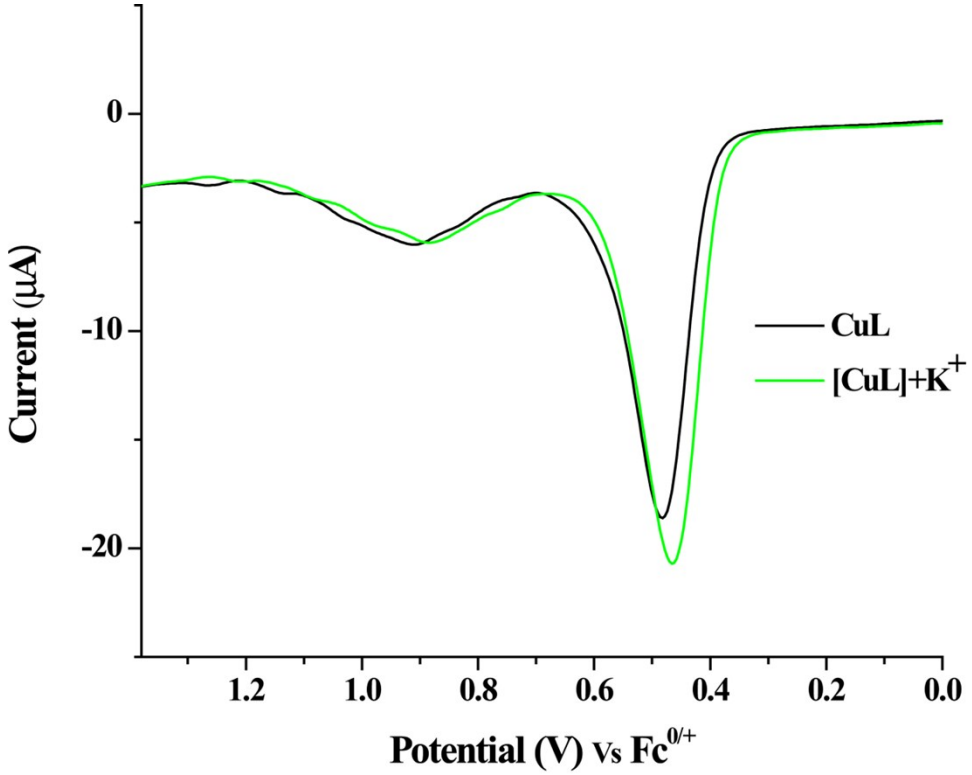

Fig. S12. Differential pulse voltametric (DPV) analysis of unbound [CuL] and [CuL]+K^+.

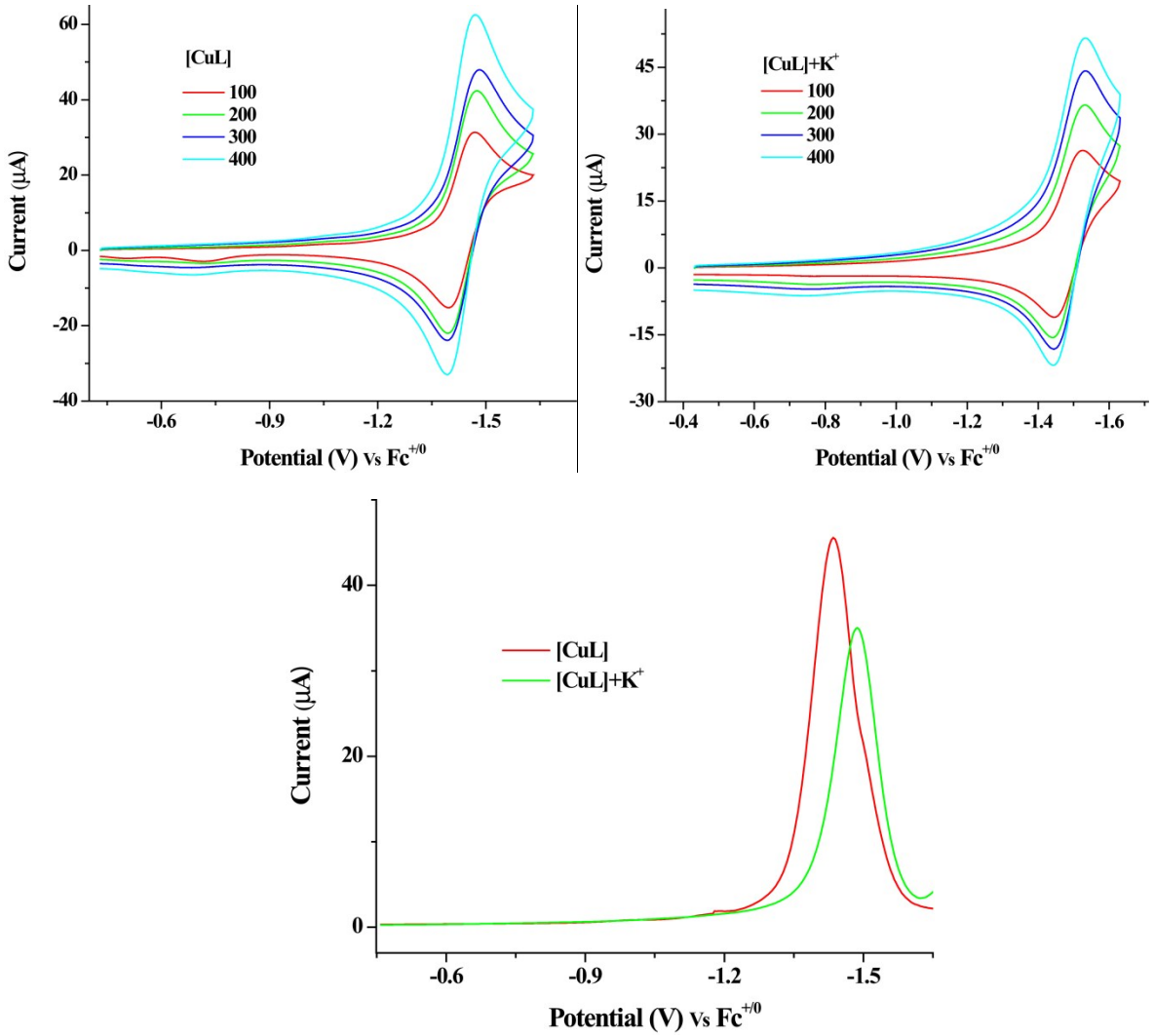

Fig. S13. Cyclic voltammograms of electrochemical reduction of unbound [CuL] (upper panel left side) and [CuL] + 10 equiv of KPF_6 (upper panel right side) in acetonitrile at multiple scan rate (mVS^{-1}) and Differential pulse voltametric (DPV) analysis of unbound [CuL] and $[CuL]+K^+$(lower panel) at a scan rate of 20 mVS^{-1}.

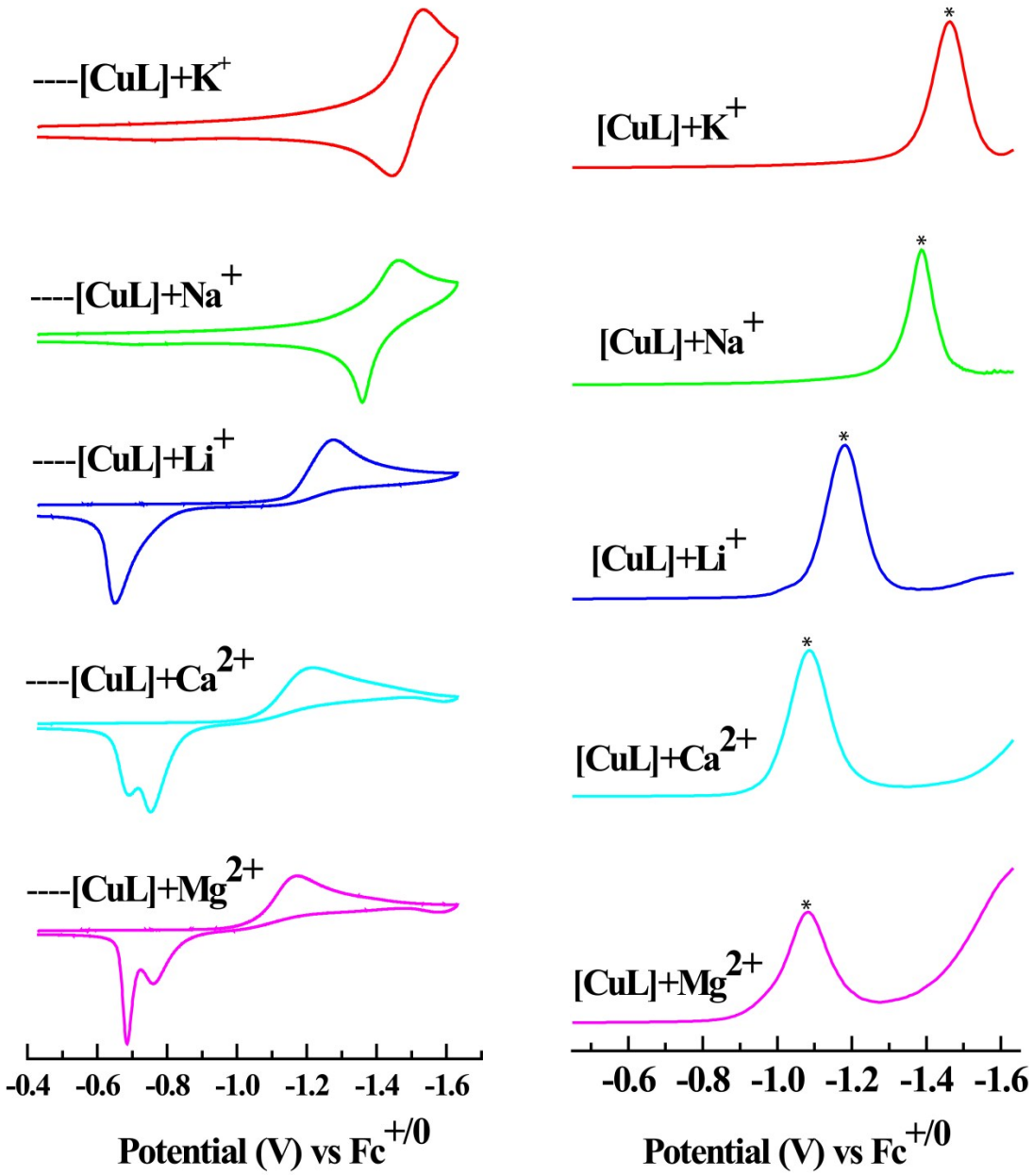

Fig. S14. Left Panel: Cyclic voltammograms of Cu(II/I) couple in presence of 10 equiv of specified redox-inactive metal ions in acetonitrile at a scan rate of 300 $mV.s^{-1}$. Right panel: DPV analysis of the corresponding mixtures at a scan rate of 20 $mV.s^{-1}$.

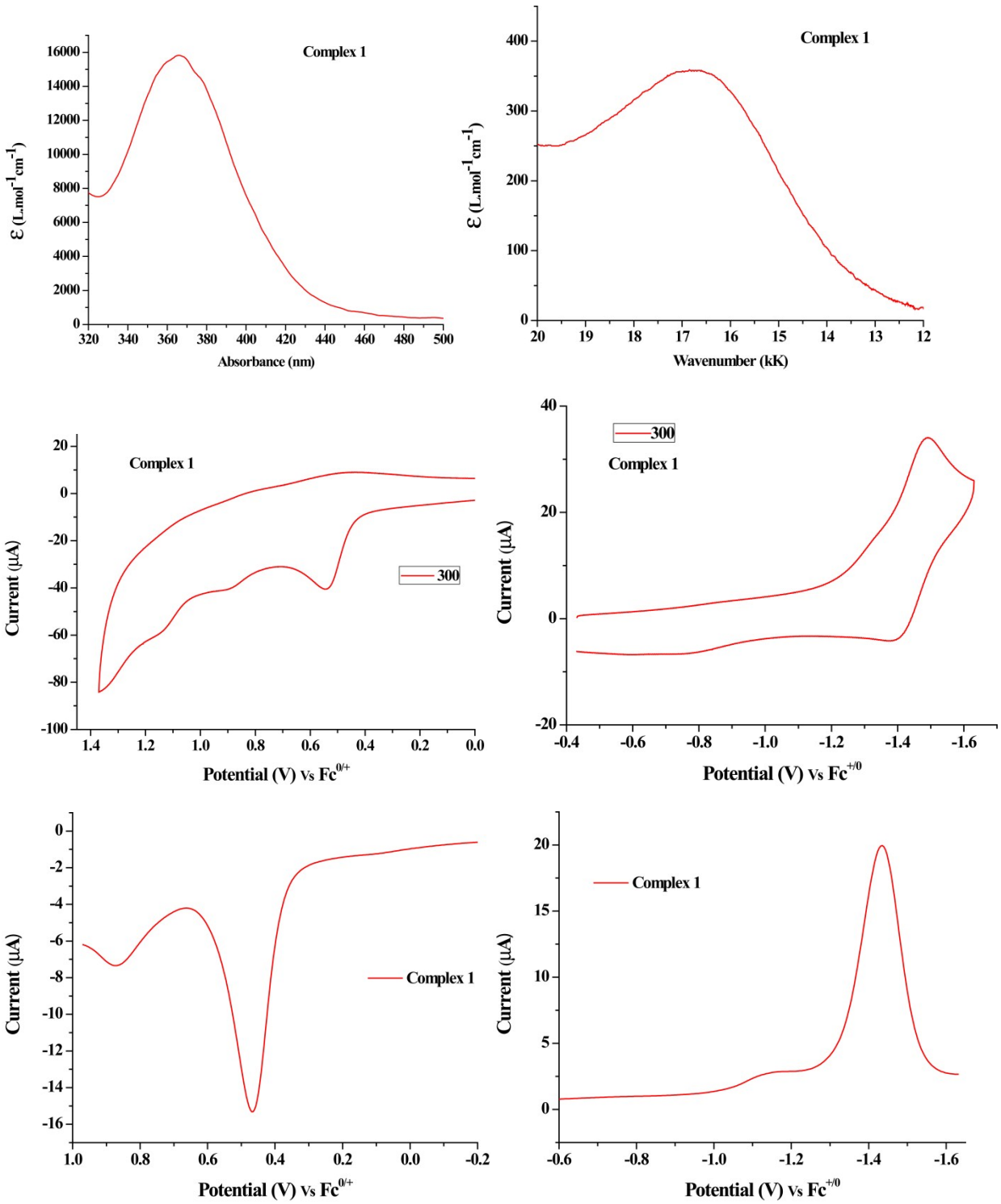

Fig. S15. Top: UV-VIS spectra, Middle: CV (300 mV.s^{-1} scan rate) and Bottom: DPV (20 mV.s^{-1} scan rate) of complex **1** at different potential range in presence of 100 equiv of TBAHFP in acetonitrile.

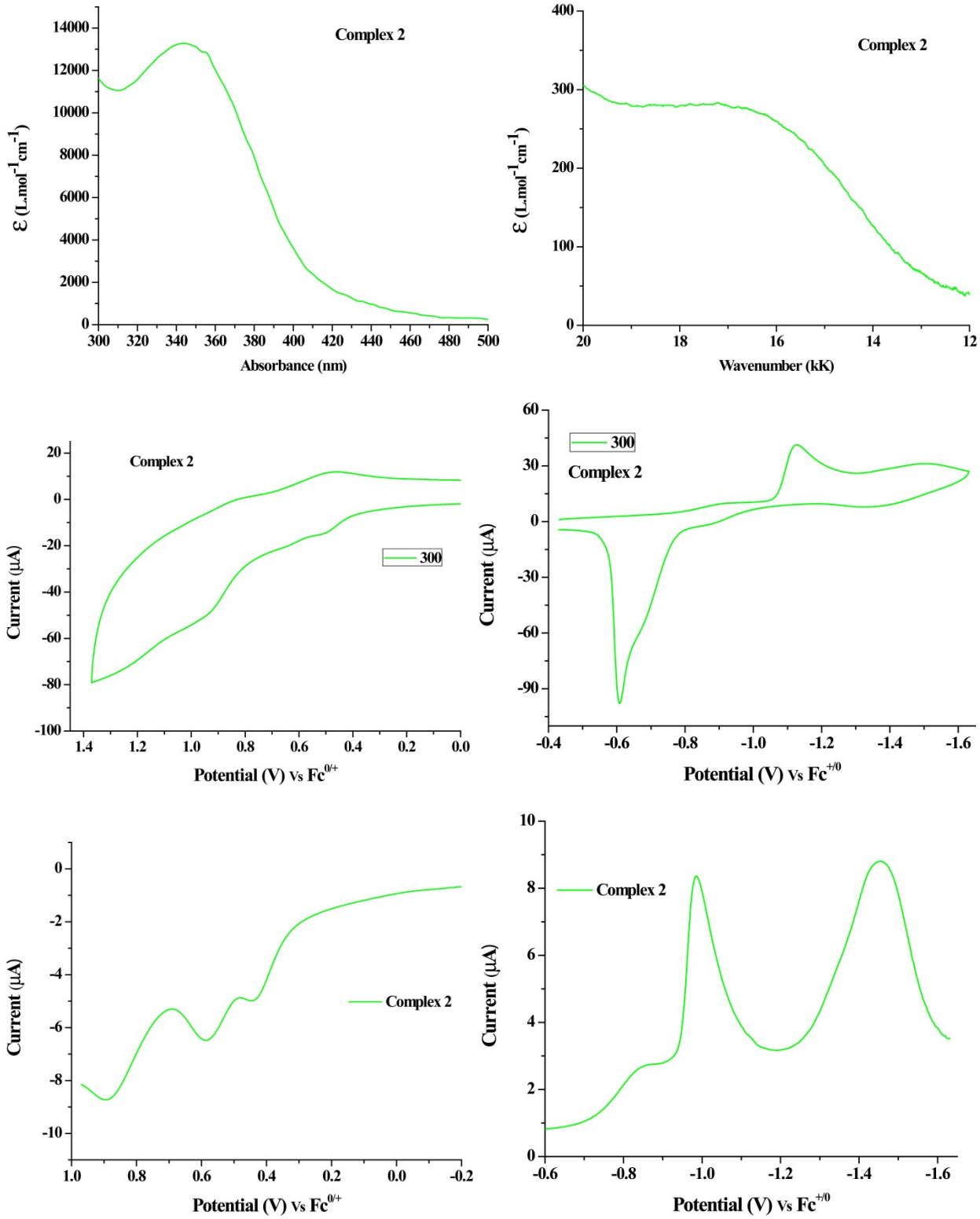

Fig. S16. Top: UV-VIS spectra, Middle: CV (300 mV.s^{-1} scan rate) and Bottom: DPV (20 mV.s^{-1} scan rate) of complex **2** at different potential range in presence of 100 equiv of TBAHFP in acetonitrile.

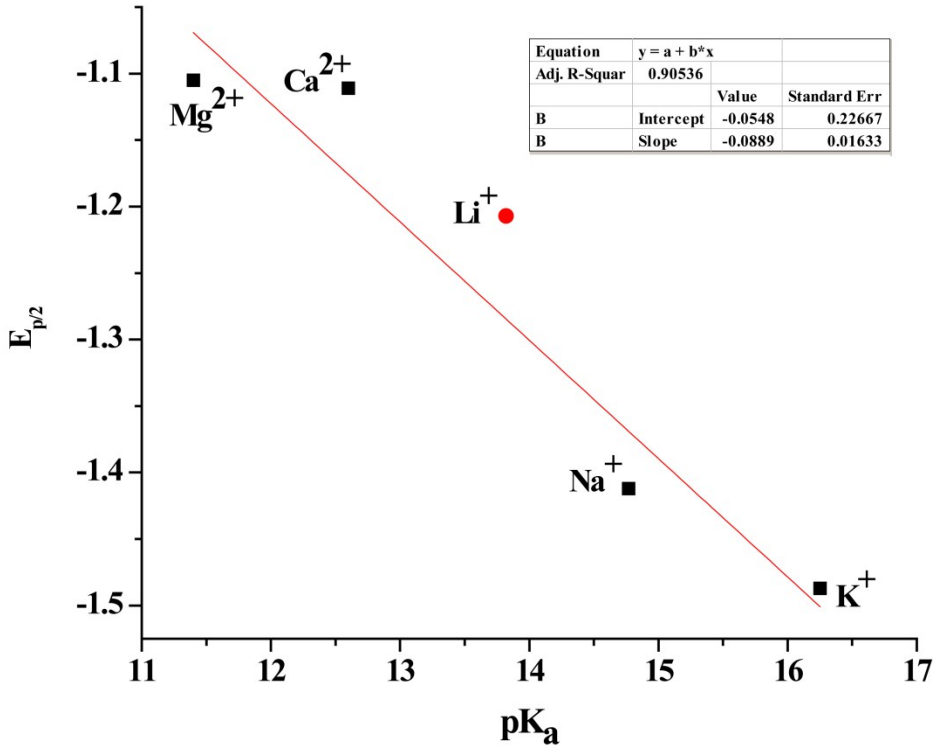

Fig. S17. Dependence of half-wave potentials ($E_{1/2}$) of electrochemical reduction of the heterometallic complexes ($[(CuL)M']^{n+}$) *vs.* pK_a of M'(aqua)$^{n+}$ ions as measure of their Lewis acidity.

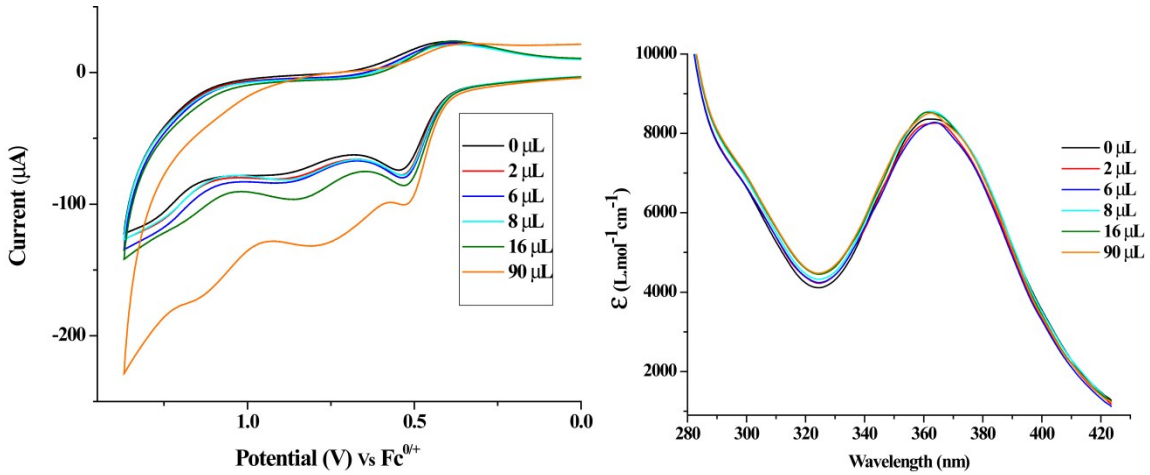

Fig. S18. Electrochemical response of [CuL] in acetonitrile upon incremental addition of aquous acetonirile (left) and the corresponding change in molar extinction coefficient of LMCT band (right).

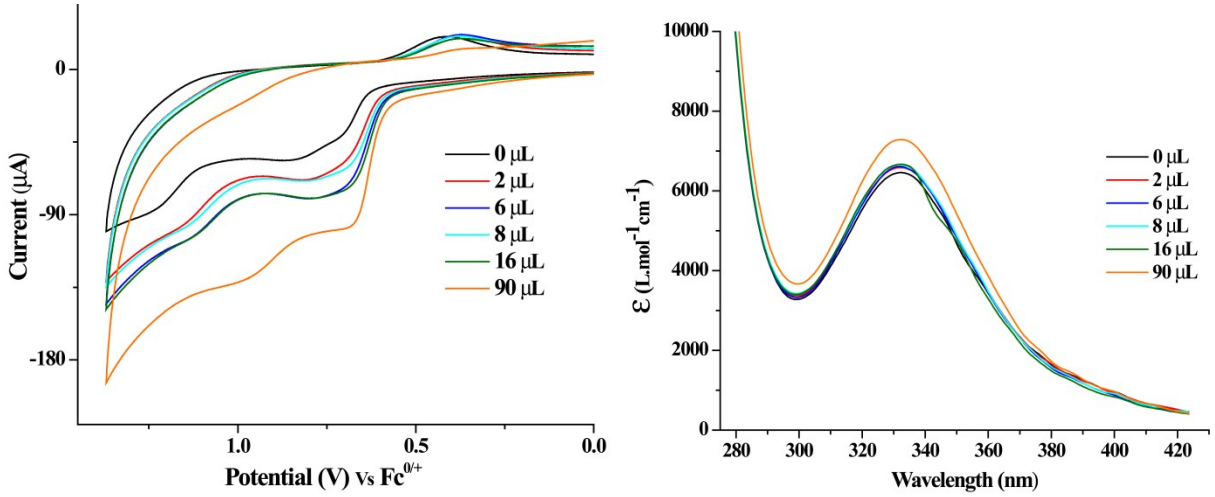

Fig. S19. Electrochemical response of [CuL] + 10 eqv. Zn^{2+} in acetonitrile upon incremental addition of aquous acetonirile (left) and the corresponding change in molar extinction coefficient of LMCT band (right).

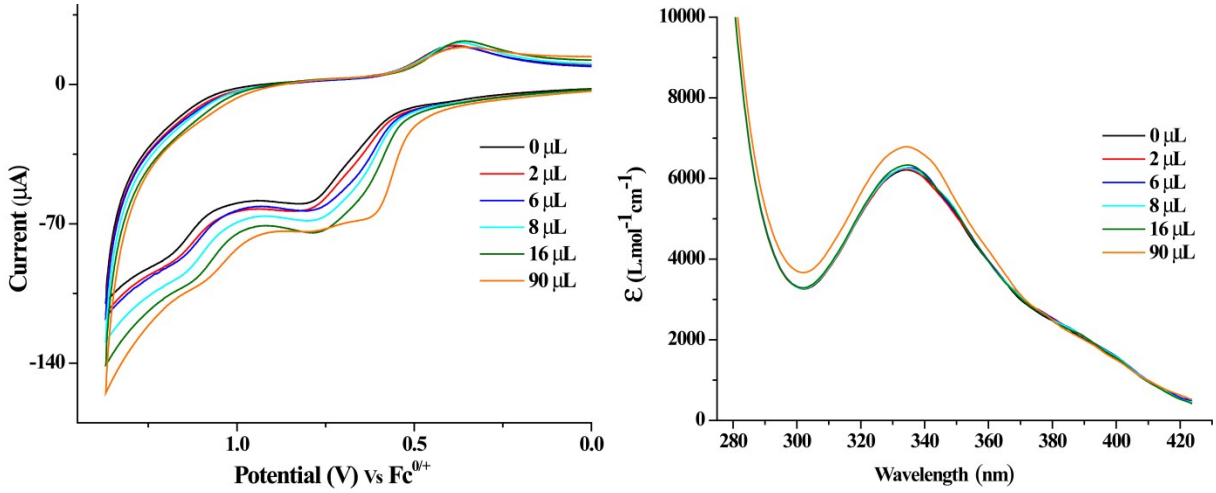

Fig. S20. Electrochemical response of [CuL] + 10 eqv. Mg^{2+} in acetonitrile upon incremental addition of aquous acetonirile (left) and the corresponding change in molar extinction coefficient of LMCT band (right).

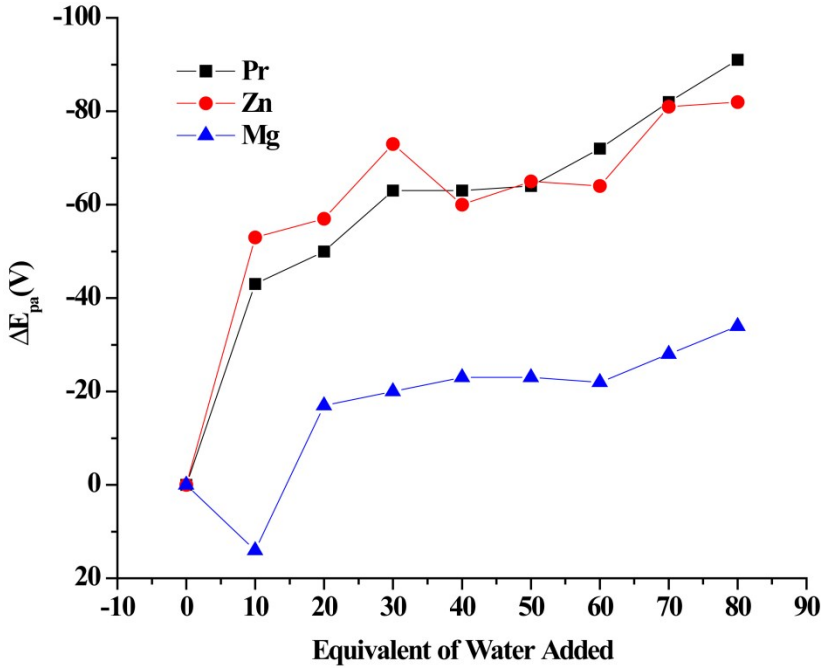

Fig. S21. Correlation of shift of oxidation peak potential with equivalent of water added for [CuL]+M'^{n+}(M'^{n+} = Pr^{3+}, Zn^{2+}, Mg^{2+}). (Solid line is guide for eye)

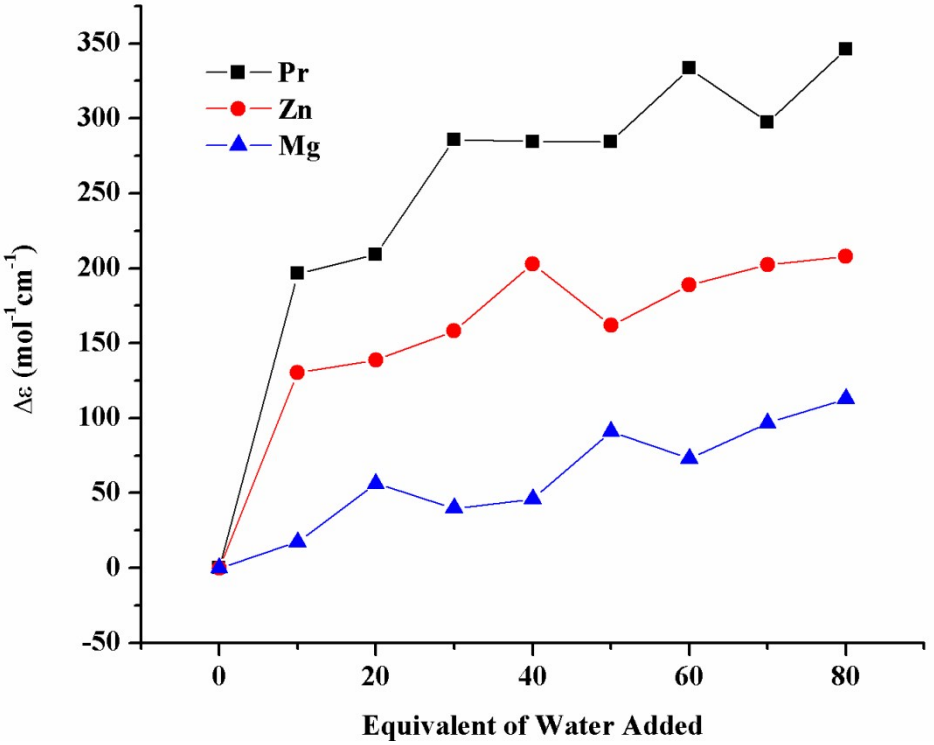

Fig. S22. Correlation of change of molar absorptivity with equivalent of water added for [CuL]+M'^{n+}(M'^{n+} = Pr^{3+}, Zn^{2+}, Mg^{2+}). (Solid line is guide for eye)

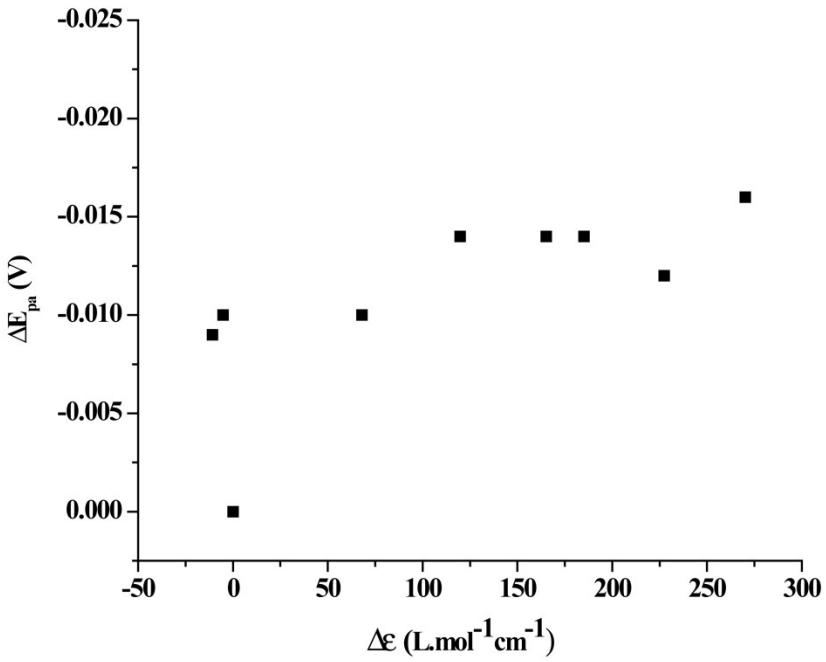

Fig. S23. Correlation of the shift of oxidation peak potential with the change of molar extinction coefficient of [CuL] in acetonitrile upon incremental addition of aquous acetonirile.

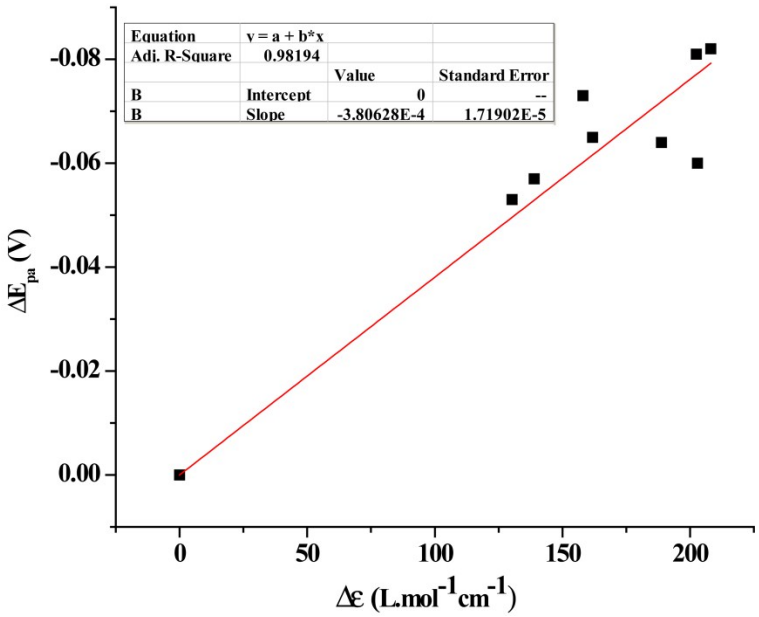

Fig. S24. Correlation of the shift of oxidation peak potential with the change of molar extinction coefficient of [CuL]+10 eqv. Zn^{2+} in acetonitrile upon incremental addition of aquous acetonirile.

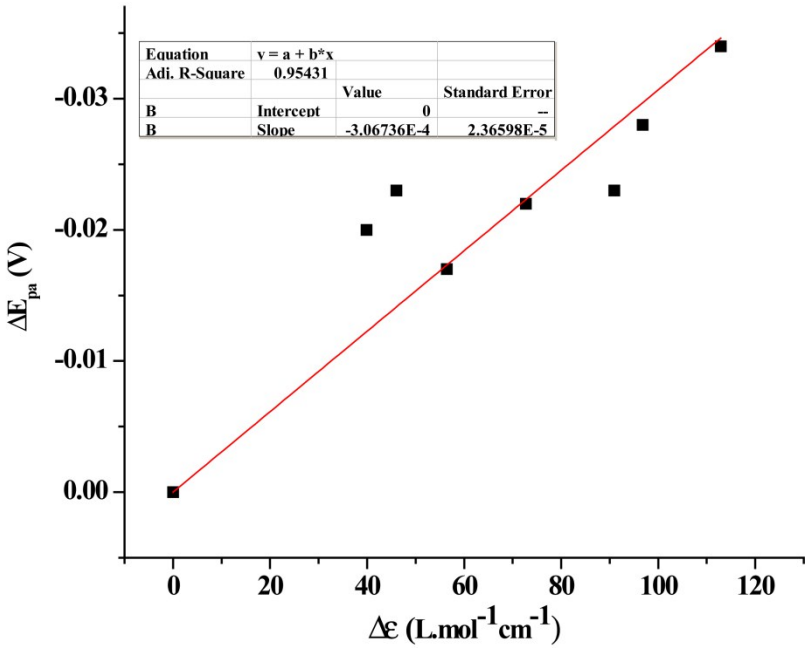

Fig. S25. Correlation of the shift of oxidation peak potential with the change of molar extinction coefficient of [CuL]+10 eqv. Mg^{2+} in acetonitrile upon incremental addition of aquous acetonirile.

Table S1. List of bond lengths (Å) and bond angles (º) of complexes **1** and **2**.

	M = **K**	M = **Zn**
M(1)–O(1)	2.020(6)	2.000(4)
M(1)–O(2)	2.179(5)	2.279(5)
M(1)–O(3)	2.012(5)	1.986(4)
M(1)–O(4)	2.184(6))	2.345(5)
M(1)–O(5)	2.058(6)	2.062(5)
M(1)–O(6)	2.037(5)	2.031(5)
Cu(1)–O(1)	1.920(5)	1.909(5)
Cu(1)–O(2)	1.944(4)	1.917(4)
Cu(1)–N(1)	2.004(6)	1.982(6)
Cu(1)–N(2)	1.937(7)	1.913(6)
Cu(2)–O(3)	1.909(5)	1.922(5)

Cu(2)–O(4)	1.937(5)	1.896(4)
Cu(2)–N(3)	1.966(5)	1.963(5)
Cu(2)–N(4)	1.933(7)	1.927(5)
O(1)–M(1)–O(2)	74.48(18)	71.82(17)
O(1)–M(1)–O(3)	156.7(2)	148.31(19)
O(1)–M(1)–O(4)	89.1(2)	84.56(17)
O(1)–M(1)–O(5)	102.0(2)	106.1(2)
O(1)–M(1)–O(6)	94.2(2)	95.4(2)
O(2)–M(1)–O(3)	87.38(19)	84.00(18)
O(2)–M(1)–O(4)	81.3(2)	77.19(17)
O(2)–M(1)–O(5)	92.9(2)	94.41(18)
O(2)–M(1)–O(6)	168.4(2)	166.16(18)
O(3)–M(1)–O(4)	73.4(2)	70.02(16)
O(3)–M(1)–O(5)	93.3(2)	95.63(19)
O(3)–M(1)–O(6)	102.8(2)	105.8(2)
O(4)–M(1)–O(5)	165.7(2)	163.85(18)
O(4)–M(1)–O(6)	96.3(2)	96.75(18)
O(5)–M(1)–O(6)	91.9(2)	94.3(2)
O(1)–Cu(1)–O(2)	82.4(2)	82.38(18)
O(1)–Cu(1)–N(1)	90.5(2)	90.2(2)
O(1)–Cu(1)–N(2)	169.3(3)	169.0(2)
O(2)–Cu(1)–N(1)	163.3(2)	165.6(2)
O(2)–Cu(1)–N(2)	91.8(3)	92.0(2)
N(1)–Cu(1)–N(2)	97.4(3)	97.3(2)
O(2)–Cu(2)–O(3)	70.47(16)	69.93(16)
O(2)–Cu(2)–O(4)	68.4(2)	70.92(17)
O(2)–Cu(2)–N(3)	98.2(2)	96.83(17)
O(2)–Cu(2)–N(4)	113.4(2)	114.92(18)

O(3)–Cu(2)–O(4)	81.5(2)	81.90(18)
O(3)–Cu(2)–N(3)	90.3(2)	90.1(2)
O(3)–Cu(2)–N(4)	171.2(2)	171.7(2)
O(4)–Cu(2)–N(3)	166.0(3)	167.1(2)
O(4)–Cu(2)–N(4)	92.5(3)	93.2(2)
N(3)–Cu(2)–N(4)	96.8(3)	95.9(2)

Table S2. Correlation of electrochemical response of previously reported 1:1 metallohost : redox-inactive ion adducts derived from bicompartmental macrocyclic ligands containing adjacent N_2O_2 and 18-crown-6 like cavity with pK_a of corresponding metal-aqua complex.

[MnL](PF$_6$)+MX$_n$ in acetonitrile, MX$_n$ =	pK$_a$	E$_{1/2}$ for Mn(III/II) (V *vs.* SCE)
KPF_6	16.25	0.025
$LiClO_4$	13.82	0.055
$Ba(OTf)_2$	13.36	0.200
$Ca(OTf)_2$	12.60	0.245
Li^+(expected)		0.176
[Li^+(experimental) - Li^+(expected)]		0.055 - 0.176 = -0.121

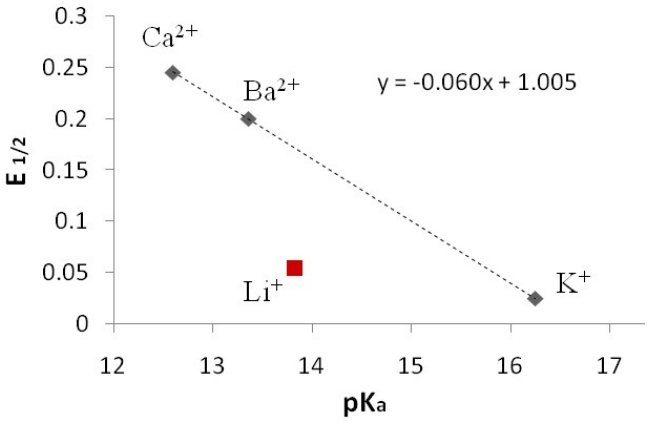

Data plotted from reference [16] of the main text.

[NiL]+MX$_n$ in acetonitrile, MX$_n$ =	pK$_a$	E$_{PC}$ for Ni(II/I) (V *vs.* ferrocene)
$NaPF_6$	14.77	-1.65
$Ca(OTf)_2$	12.60	-1.42
$Nd(OTf)_3$	8.43[a]	-1.18
$Y(OTf)_3$	8.04[a]	-1.22
Y^{3+}(expected)		-1.13
[Y^{3+}(experimental) - Y^{3+}(expected)]		-1.22-(-1.13) = -0.09
[a]obtained from ref		

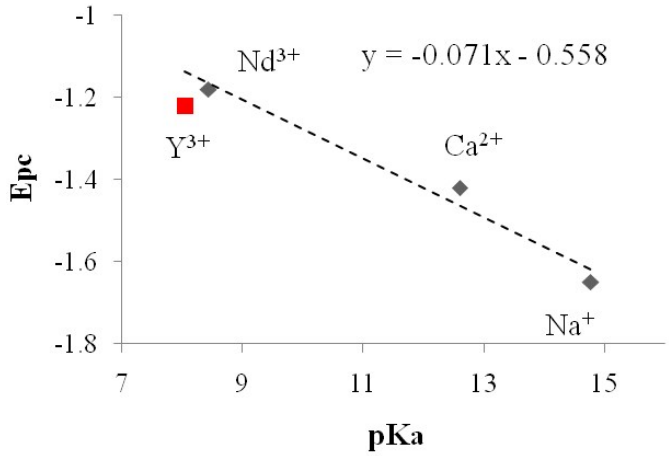

Data plotted from reference [17] of the main text.

[56] of main text			
[CoL] + MX_n in DMF, MX_n =	pK_a	$E_{1/2}$ for Co(II/I) (V *vs.* ferrocene)	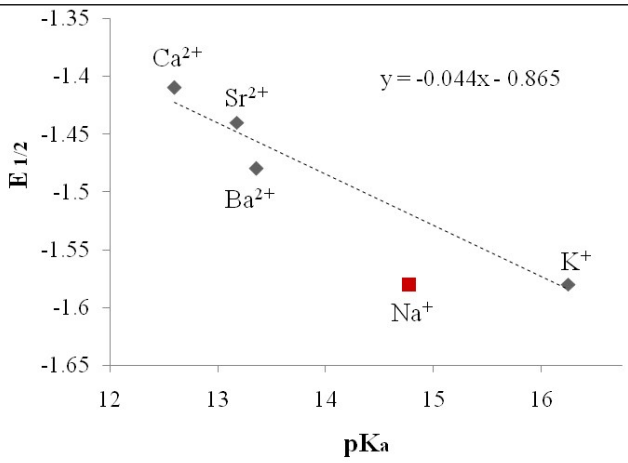
K(OTf)	16.25	-1.58	
Na(OTf)	14.77	-1.58	
$Ba(OTf)_2$	13.36	-1.48	
$Sr(OTf)_2$	13.18	-1.44	
$Ca(OTf)_2$	12.60	-1.41	
Na^+(expected) [Na^+(experimental) - Na^+(expected)]		-1.515 -1.58 - (-1.515)= -0.065	
			Data plotted from reference [18] of the main text.
[CuL]+M^{n+} in DMSO, M^{n+}=	pK_a	$E_{1/2}$ for Cu(II/I) (V *vs.* Ag/AgCl)	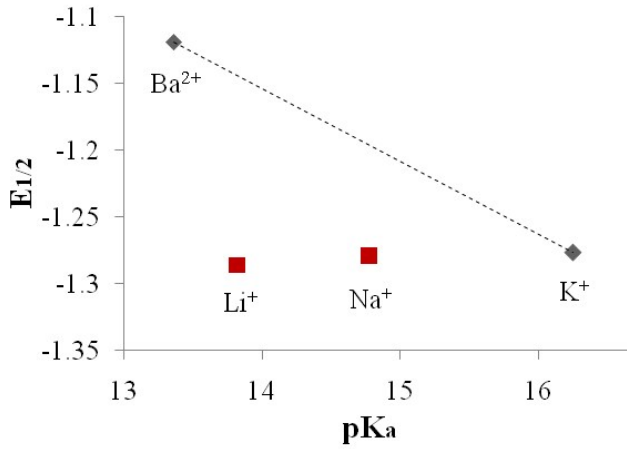
K^+	16.25	-1.277	
Na^+	14.77	-1.279	
Li^+	13.82	-1.286	
Ba^{2+}	13.36	-1.119	
Na^+(expected) [Na^+(experimental) - Na^+(expected)]		-1.185 -1.279-(-1.185)= -0.094	
Li^+(expected) [Li^+(experimental) - Li^+(expected)]		-1.134 -1.286-(-1.134)= -0.152	
			Data plotted from reference [19] of the main text. Line is guide for eye.
[Mn(N)L] + MX_n in acetonitrile, MX_n =	pK_a	$E_{1/2}$ for Mn(V/VI) (V *vs.* ferrocene)	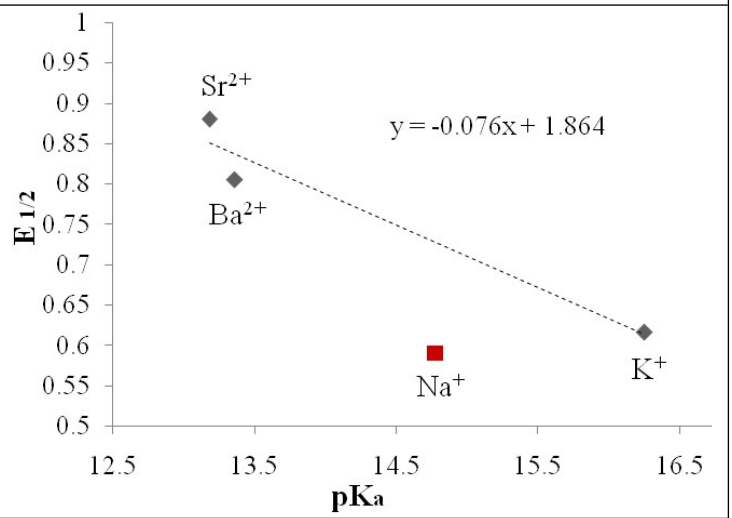
K(OTf)	16.25	0.616	
Na(OTf)	14.77	0.591	
$Ba(OTf)_2$	13.36	0.805	
$Sr(OTf)_2$	13.18	0.880	
Na^+(expected) [Na^+(experimental) - Na^+(expected)]		0.723 0.591-0.723 = -0.132	
			Data plotted from reference [31] of the main text.

Table S3. Masses of species obtained with their calculated values.

[CuL]+ 10 eqv. $M'X_n$ salts	Figure	Species detected with charge	Experimental Mass (*m/z*)	Calculated Mass (*m/z*)	[CuL]:M′
$Li(ClO_4).3H_2O$	S3	$[(CuL)_2Li]^+$	721.16	721.14	2:1
		$[(CuL)Li]^+$	364.07	364.08	1:1
$Zn(ClO_4)_2.6H_2O$	S4	$[(CuL)_2Zn(ClO_4)]^+$	877.01	877.01	2:1
		$[(CuL)_2Zn]^{2+}$	390.03	390.03	2:1
		$[(CuL)Zn(ClO_4)]^+$	519.94	519.94	1:1
$Cd(ClO_4)_2.6H_2O$	S5	$[(CuL)_2Cd(ClO_4)]^+$	926.98	926.98	2:1
		$[(CuL)_2Cd]^{2+}$	414.02	414.01	2:1
		$[(CuL)Cd(ClO_4)]^+$	569.91	569.91	1:1
$Pr(NO_3)_3{\cdot}6H_2O$	S6	$[(CuL)_2Pr(NO_3)_2]^+$	979.03	979.02	2:1
		$[(CuL)Pr(NO_3)_2]^+$	621.96	621.96	1:1
$Nd(NO_3)_3{\cdot}6H_2O$	S7	$[(CuL)_2Nd(NO_3)_2]^+$	980.01	980.01	2:1
		$[(CuL)Nd(NO_3)_2]^+$	622.95	622.94	1:1
$Sm(NO_3)_3{\cdot}6H_2O$	S8	$[(CuL)_2Sm(NO_3)_2]^+$	990.02	990.02	2:1
		$[(CuL)Sm(NO_3)_2]^+$	632.96	632.96	1:1

Table S4. Comparison of HOMO-LUMO gap with the overall electrochemical shift in 1:1 adducts.

Complex	**Relative stabilization of HOMO-LUMO gap ($\Delta\lambda_{max}$) with respect to [CuL]+K^+ (meV)**	**Expected shift with respect to [CuL]+K^+** $\frac{meV}{1\,e} = mV$	**[$E_{1/2}$ (ox) - $E_{1/2}$ (red)] =$\Delta E_{1/2}$ observed from DPV (V)**	**Relative shift of $\Delta E_{1/2}$ with respect to [CuL]+K^+ (mV)**
[CuL]+K^+	(9.43-9.43)	= 0	0.466-(-1.487) =1.953	1.953-1.953 = 0
[CuL]+Na^+	(48.68-9.43)	= 39.25	0.487-(-1.412) =1.899	1.953-1.899 = 54
[CuL]+Li^+	(199.20-9.43)	= 189.77	0.555-(-1.207) = 1.762	1.953-1.762 = 191
[CuL]+Ca^{2+}	(258.07-9.43)	= 248.64	0.589-(-1.111) = 1.700	1.953-1.700 = 253
[CuL]+Mg^{2+}	(285.43-9.43)	= 276.00	0.623-(-1.107) = 1.730	1.953-1.730 = 223

Table S5. Summary of UV-Vis and electrochemical properties of complexes **1** and **2**.

	Complex **1**	[CuL]+10 equiv K^+	Complex **2**	[CuL]+10 equiv Zn^{2+}
λ_{max} (LMCT) nm	365.5	362	344 nm	332.5
$E_{1/2}$ (ox) (V) from DPV	0.493, 0.898	0.466, 0.913	0.471, 0.612, 0.920	0.652, 0.784
$E_{1/2}$ (red) (V) from DPV	-1.175 (hump), -1.459	-1.487	-0.875 (hump), -1.011, -1.477	Not done